AC SAF VALIDATION REPORT

Validated products:

Name	Satellite(s)
IASI CO L3 CDR and ICDR O3M-543 and 359	Metop-A, B, C

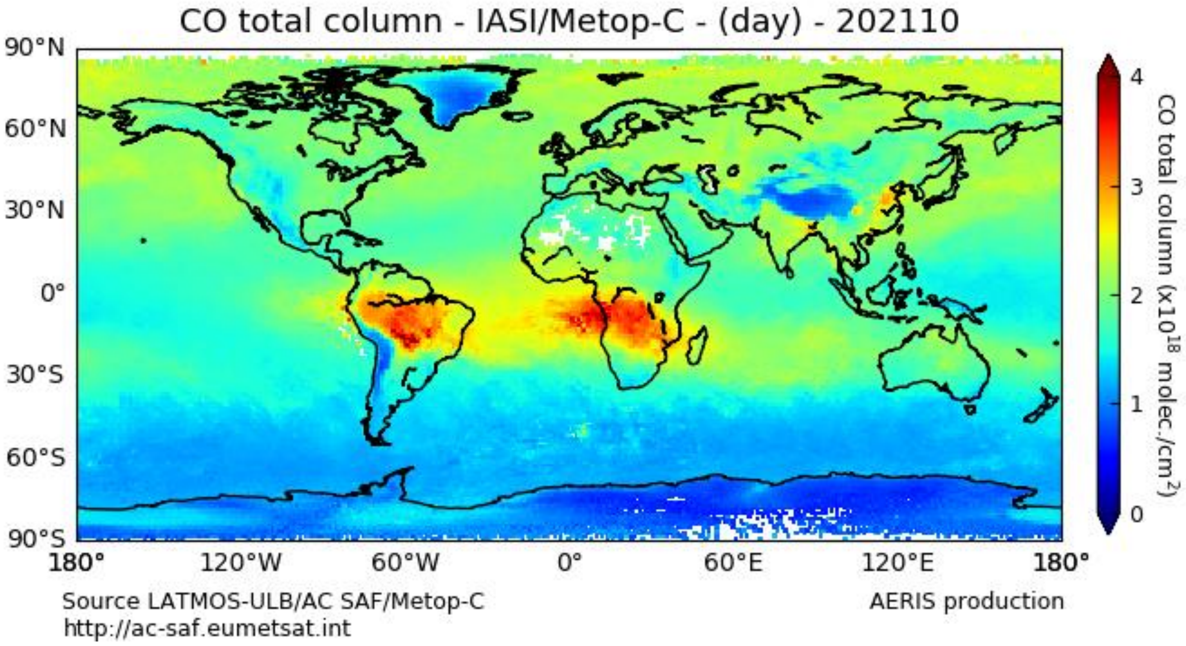

Authors:

Name	Institute
Maya George Sarah Safieddine Cathy Clerbaux	LATMOS, France
Rosa Astoreca Daniel Hurtmans Pierre-François Coheur	ULB, Belgium

Reporting period: 2008 – 2021

Input data versions: IASI/Metop NRT EumetCAST BUFR_IASI_COx 6.5

Data processor versions: NA

Table of contents

1. INTRODUCTION

1.1 Carbon monoxide CDR and ICDR

Carbon monoxide (CO) is one of the most important precursors of ozone and an important trace gas for the understanding of both air quality and climate forcing. Because of its relatively long lifetime (a few weeks to a few months depending on latitude and time of year), CO is one of the main tracers of long-range transport of pollution. Formed by the incomplete combustion of fossil and bio-fuels, and by vegetation burning, CO is also produced in the atmosphere via the oxidation of methane and non-methane hydrocarbons by the hydroxyl radical (OH). It is the largest global sink of the OH radical and thus plays an important role in the oxidizing power of the atmosphere and in the concentrations of greenhouse gases.

In this validation report, we use the **CO climate data record or CDR** (with the AC-SAF nomenclature O3M-543) **for Metop A and Metop B**. EUMETSAT reprocessed the whole IASI CO data record between 2020 and 2021 and the CO CDR are available until December 2021. This was done to account for algorithm updates and to make the whole time series of IASI-CO, for the first time, homogeneous. Metop C data (2019 onwards) is supposed to be running with the latest algorithm, and as such was not included in the reprocessing exercise. The notation **"interim"** climate data record, **or ICDR** (with the AC-SAF nomenclature O3M-359) is used to account for all CO products produced outside the CDR reprocessing exercise, i.e. **the time series of IASI on Metop C (2019 onwards).**

1.2 Purpose and data

This validation report (VR) aims at validating IASI CO CDR L3 products by comparing them to those from MOPITT.

MOPITT CO L3 total column products are available in netcdf format through the NASA Earthdata website (https://earthdata.nasa.gov/). We used version 8 Thermal Infrared (TIR) daytime retrievals (Deeter et al., 2019 and Buchholz et al., 2021). At the time of the writing of this paper, we excluded version 9 data as only beta version is available from April 2021.

The IASI CO Level 3 products consist of monthly grids (1°x1°) and are produced from:

1- the IASI CO climate data record (CDR) Level 2 total column products reprocessed at EUMETSAT with the Fast Optimal Retrievals on Layers for IASI CO (FORLI-CO) algorithm (version 20151001), for Metop-A and B. FORLI-CO was developed by ULB in collaboration with LATMOS (Hurtmans et al., 2012).
2- The IASI CO interim climate data record (ICDR) Level 2 total column products retrieved in a near real at EUMETSAT with FORLI-CO.

The period covered in this validation exercise is January 2008-August 2021 for IASI-A (decommissioned in October 2021); March 2013-December 2021 for IASI-B and October 2019-December 2021 for IASI-C.

IASI CO CDR L3 products will be available in netcdf format through the Aeris data base (https://iasi.aeris-data.fr/co/).

Metop-A data are available from October 2007 to August 2021.
Metop-B data are available from March 2013 to present.
Metop-C data are available from October 2019 to present.

IASI CO CDR/ICDR L3 products include four grids (also see IASI CO L3 ATBD):

- COgridDAY (day time grid of CO),
- COgridNIGHT (night time grid of CO),
- ErrorgridDAY (grid or error, used to weight the CO day time grid) and,
- ErrorgridNIGHT (grid or error, used to weight the CO night time grid).

In this report, we will present daytime and nighttime comparison.
Note that error grids cannot be validated as they are representative of the total error from the CO total columns. However, we perform an inter-comparison between errors from the three IASI CO CDR L3 products (A, B and C) in Section 2.2.

1.3 Differences between MOPITT and IASI

The two instruments used in this study are not exactly the same. They both perform in the thermal infrared range, fly on low Earth orbit with Sun synchronous orbits. MOPITT on TERRA has a descending (ascending) node of 10:30 A.M. (10:30 P.M.), while IASI on METOP has a descending (ascending) node of 9:30 A.M. (9:30 P.M). They are close enough that the difference in the CO chemistry can be considered negligible. The main differences are listed here and will help in the discussion of the differences between the two instruments over different parts in the world:

- The number of observations and their coverage: each IASI measurement swath allows nearly global coverage in 1 to 2 days, while the MOPITT swath provides global coverage in 3–4 days (Drummond et al., 2010).
- IASI swaths ascending (or descending) tracks almost overlap near the equator. On the other hand, the MOPITT swaths are narrower leaving gaps of unmonitored regions, in particular over the Tropics (Barré et al., 2015) within a given day.
- Instrument and algorithm designs: each of the instruments have different interferometer performances, and have different spectral resolution and signal to noise ratio. Their retrieval algorithms use different a priori information for CO profiles and error covariance matrices and hence will lead different instrument sensitivity (George et al., 2015).

1.4 Acronyms

ATBD: Algorithm Theoretical Basis Documents
CDR: Climate Data Record
ICDR: Interim Climate Data Record
EUMETSAT: European Organisation for the Exploitation of Meteorological Satellites
EUMETCast: EUMETSAT multi-service data dissemination system
FORLI: Fast Optimal Retrievals on Layers for IASI
IASI: Infrared Atmospheric Sounding Interferometer
LATMOS: Laboratoire Atmosphères et Observations Spatiales
L3: Level 3
MOPITT: Measurement of Pollution in the Troposphere
VR: Validation Report
ULB: Université Libre de Bruxelles

1.5 Applicable document

IASI CO L3 ATBD SAF/AC/ULB/COL3_ATBD

IASI CO L3 RN SAF/AC/ULB/COL3_RN

IASI CO CDR L2 Validation Report

2. VALIDATION

In this section, we start by recalling the results of the IASI CO L2 Validation Report in section 2.1 and evaluate the biases against the requirements in terms of accuracy. Then we focus only on the L3 and present a spatial comparison in section 2.2. Then a comparison over different latitude bands is shown in section 2.3. Section 2.4 focus on regional and city scale comparison of CO L3. Conclusions of the study is summarized in section 3.

2.1 IASI CO CDR L2 Validation Report's results summary

IASI CO CDR L2 data, from which the L3 are calculated, have been validated by BIRA. From this, we can evaluate the FORLI-CO product requirements in terms of accuracy (Threshold accuracy: 25%; Target accuracy: 12%; Optimal accuracy: 5%, see PSRA). Comparisons between IASI CO CDR L2 and NDACC FTIR data are performed for 23 stations, both directly and with smoothing with the averaging kernels.

Table 2.2 of CO CDR L2 Validation Report show relative differences (for the comparison with the smoothed columns) ranging between -3.75% (-4.17%) for Zugspitze to 15.09% (15.01%) for Toronto, for IASI-A (B). So all biases are below the threshold accuracy of 25%. We count 21 stations for which biases are below the target accuracy of 12%, for both IASI-A and B. We count 11 stations below the optimal accuracy of 5% for IASI-A and 10 stations for IASI-B.

A similar conclusion holds for the direct comparison statistics in Table 2.1 where all biases are below the threshold accuracy of 25%: For IASI-A (B), relative differences are ranging between -3% (-2.24%) for Boulder to 13.15% (13.44%) for Arrival Heights. Out of the 23 stations, 22 are showing biases below 12%. We count 17 (16) stations with biases below 5% for IASI-A (B).

2.2 Spatial comparison

To start, seasonal global distributions for IASI-A, B and C, as well as for MOPITT are presented in Figure 1 to Figure 6. For each IASI instrument (A, B and C), as well as for daytime and nighttime measurements, we present subplots with global distributions for the four boreal seasons of the year: winter (December-January-February, “DJF”), spring (March-April-May, “MAM”), summer (June-July-August, “JJA”) and autumn (September-October-November, “SON”). The global distributions can be compared with MOPITT global distributions, averaged over the time period corresponding of the availabilities of the IASI instrument. For IASI-A, the considered time period is January 2008-August 2021. For IASI-B: March 2013-December 2021 and for IASI-C: October 2019-December 2021. In the third column are presented the relative difference with respect to MOPITT in percentages (100x(IASI-MOPITT)/MOPITT). We can appreciate the very good spatial agreement between the IASIs and MOPITT instruments. The best agreement between IASI and MOPITT CO distributions is seen over land during boreal springs and autumns. As explained in George et al. (2015), IASI CO concentrations in the Northern Hemisphere are slightly lower than MOPITT concentrations during the winter season. This is due to the differences in the a priori information used in the different retrieval algorithms, see section 1.3. Moreover, some differences are observed over desert or ice/snow areas (Antarctica, Russia and Canada) where different emissivity assumptions can lead to biases. Over the oceans, IASI CO concentrations are generally slightly larger than MOPITT, especially during the night. Further investigations over the ocean (for example that of the effect of the variable MOPITT versus the single apriori that IASI uses) is needed.

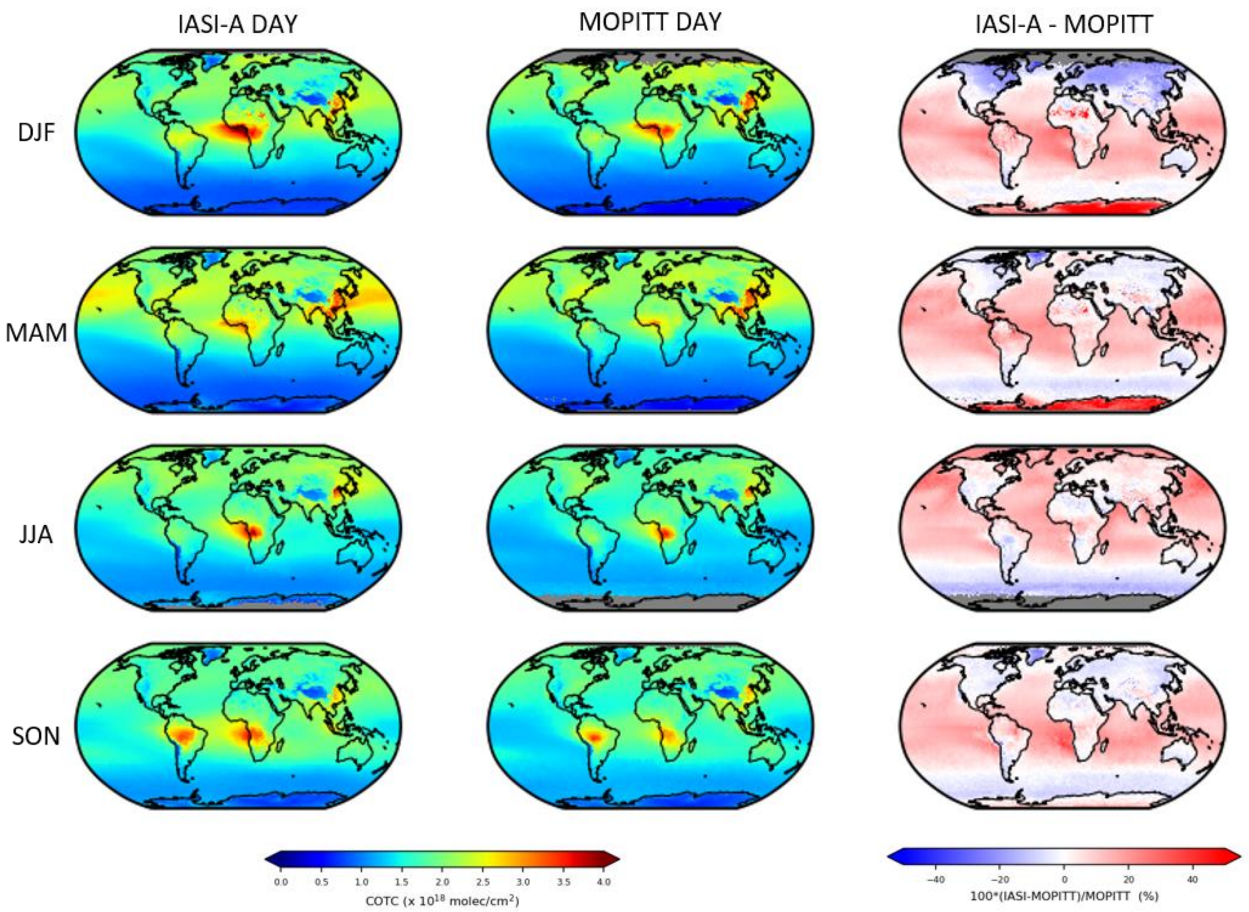

Figure 1: Daytime seasonal global distributions for IASI-A in the left column and MOPITT in the middle column. Relative differences in % are presented in the right column. Averages are performed over the “IASI-A” period: January 2008-August 2021. The boreal seasons are shown on the different rows: winter (December-January-February, “DJF”); spring (March-April-May, “MAM”), summer (June-July-August, “JJA”), and autumn (September-October-November, “SON”) on line four.

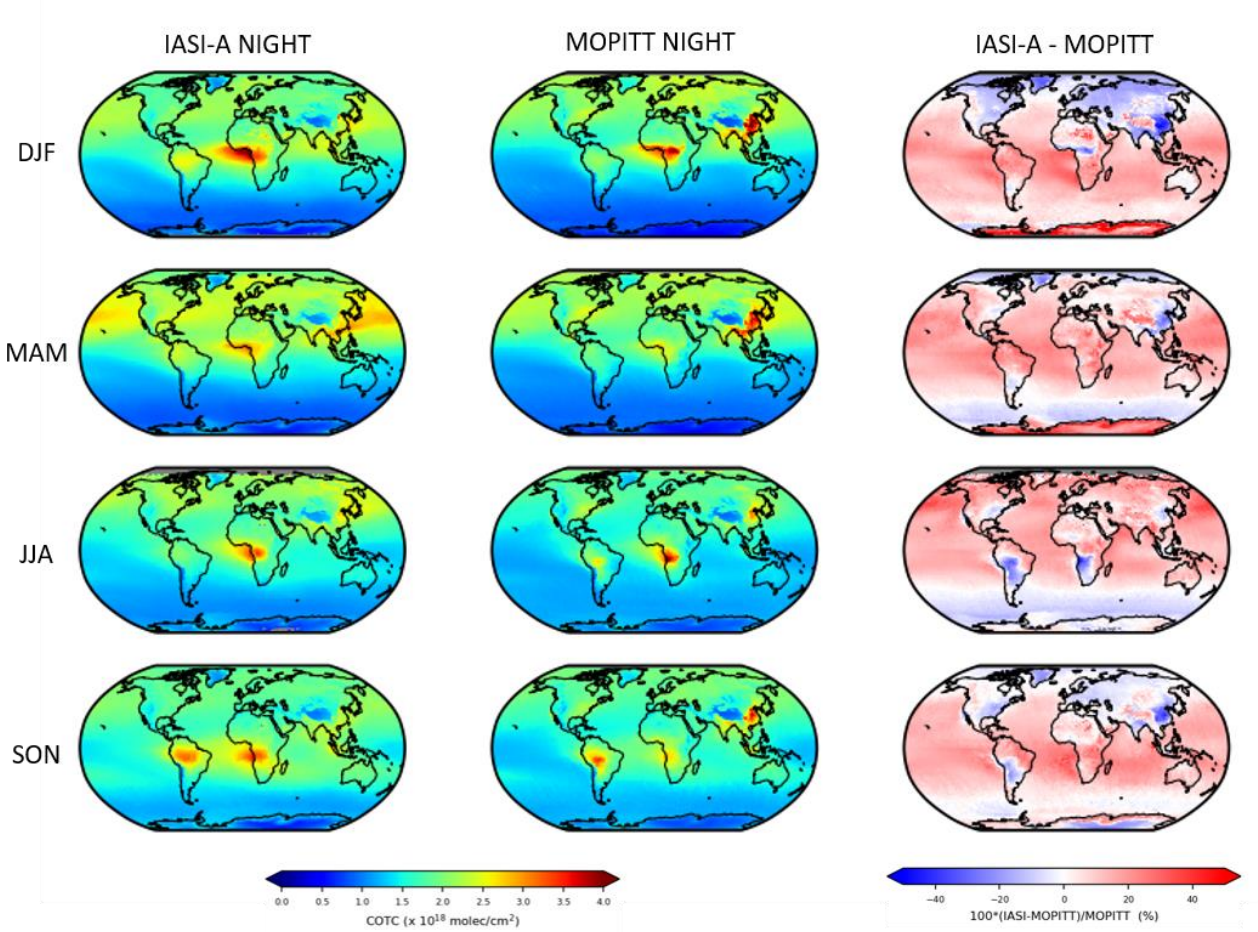

Figure 2: Same as Figure 1 but for nighttime data.

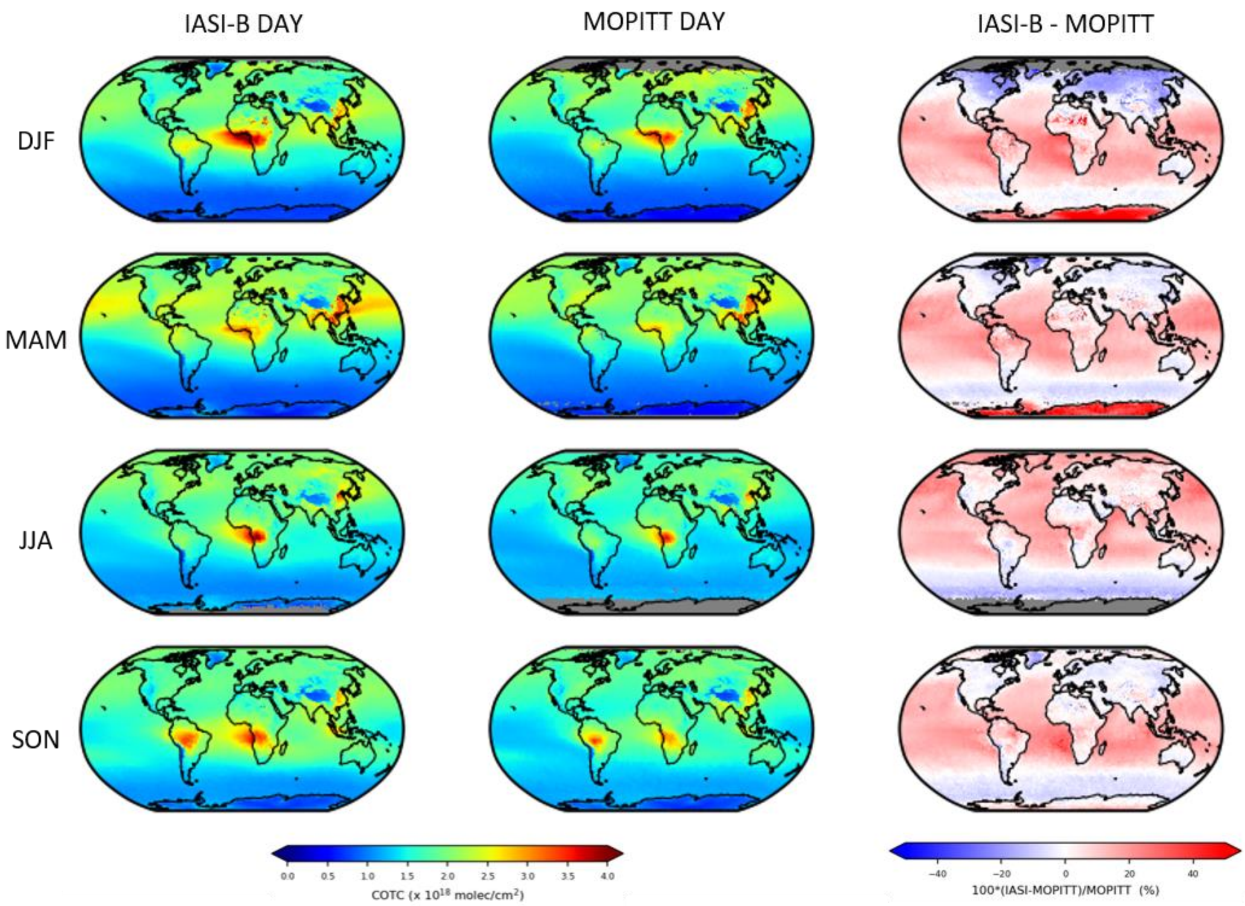

Figure 3: Same as Figure 1 but for IASI-B.

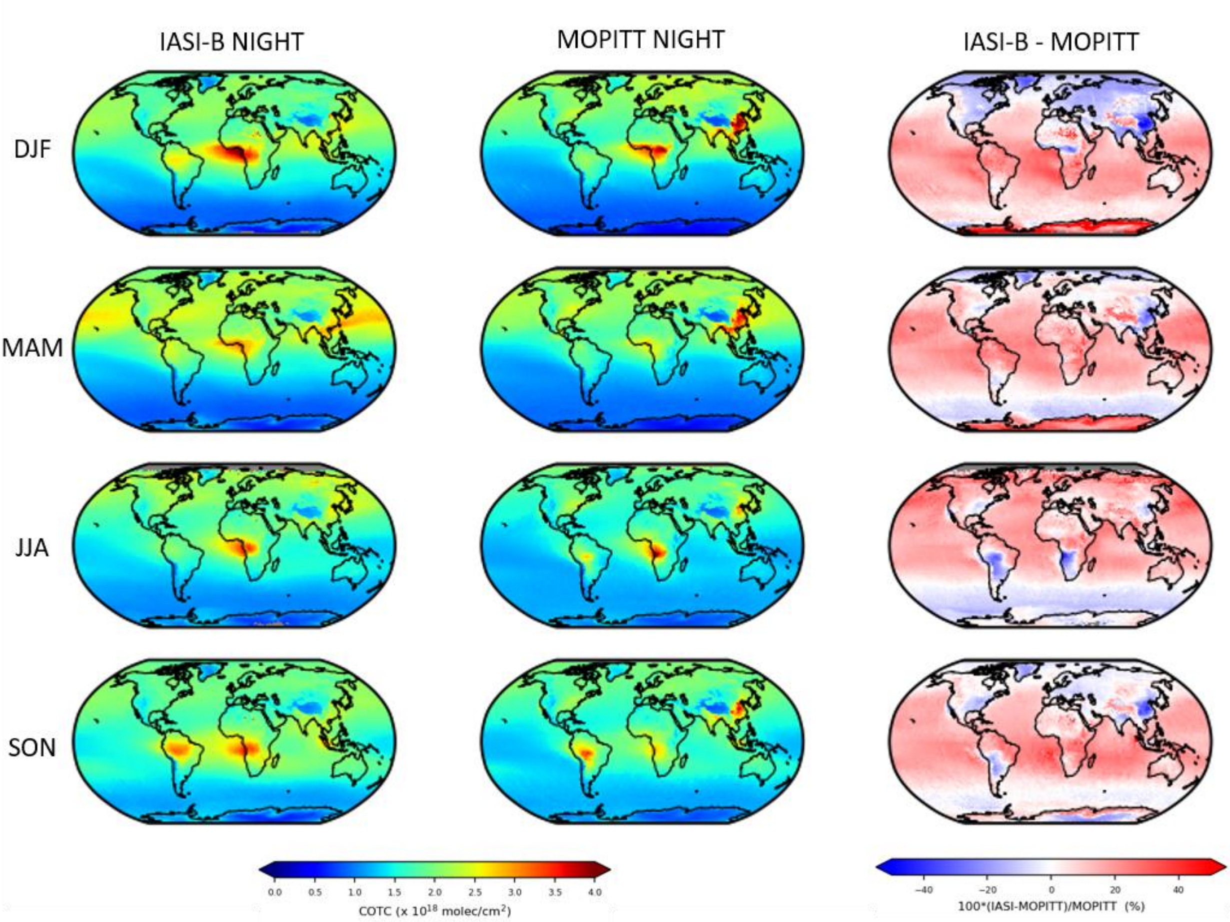

Figure 4: Same as Figure 1 but for IASI-B nighttime data.

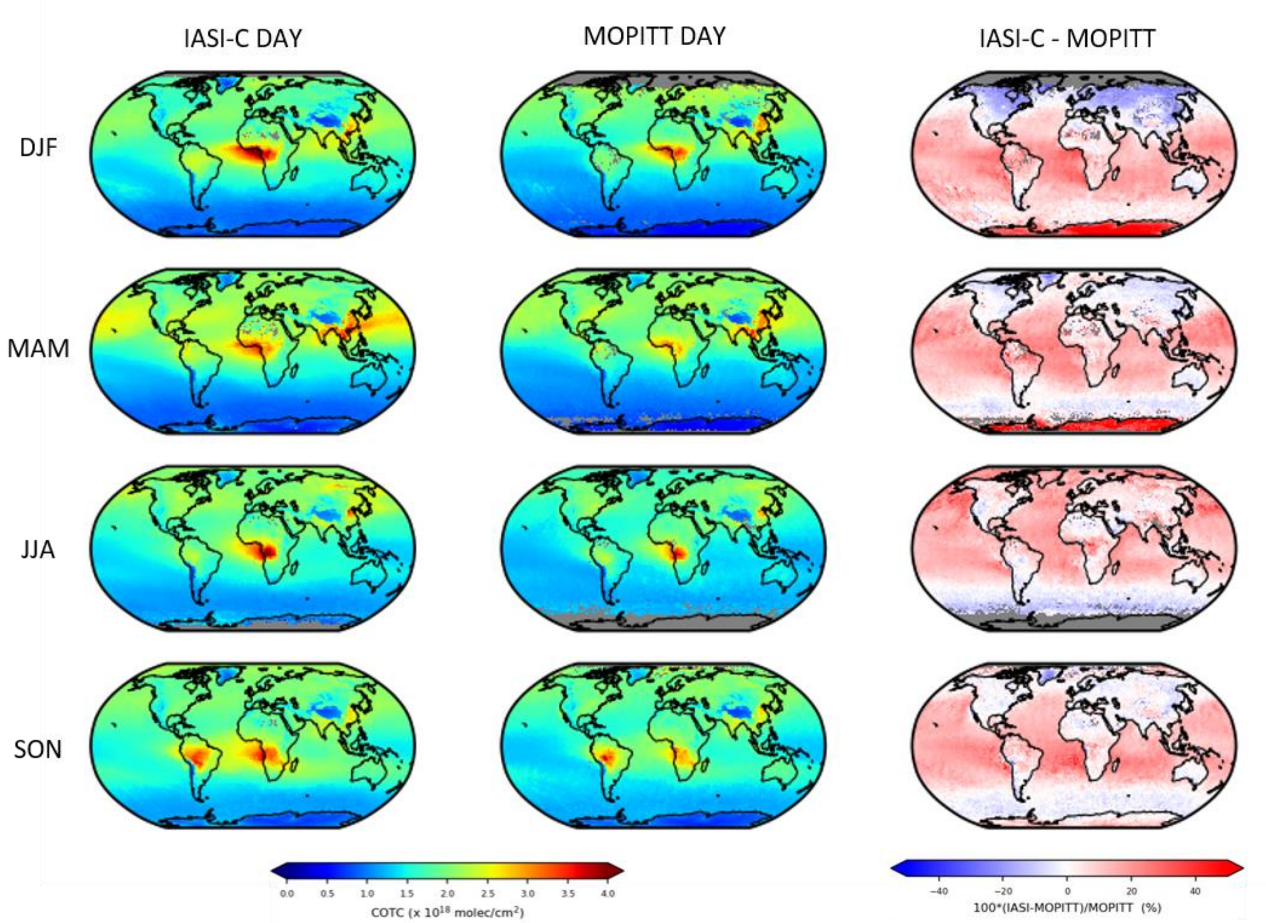

Figure 5 : Same as Figure 1 but for IASI-C.

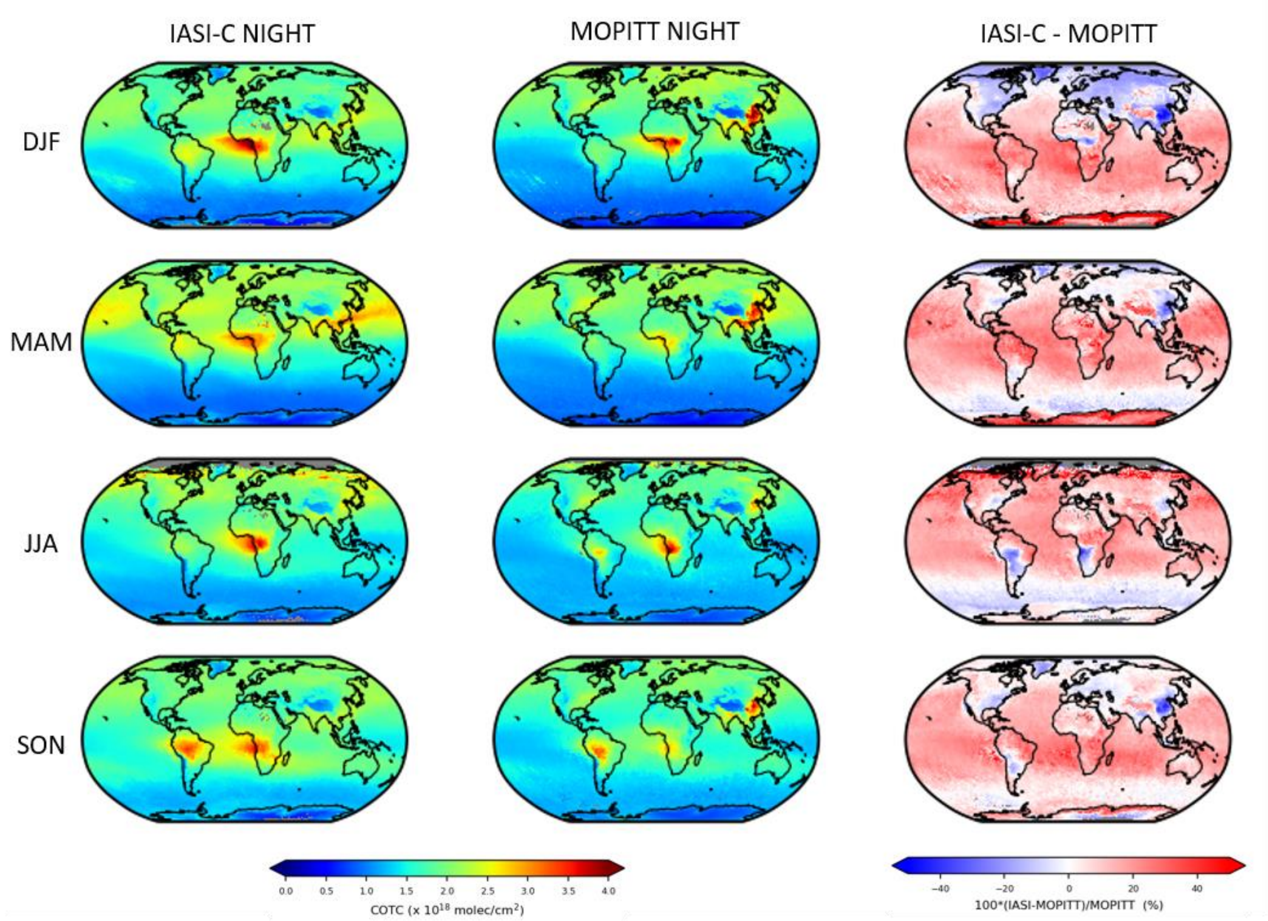

Figure 6: Same as Figure 1 but for IASI-C nighttime data.

2.3 Comparison over different latitude bands

Averages over different latitude bands are performed in Figure 7 (daytime) and Figure 8 (nighttime), for the entire globe (upper panel), for latitudes between 20° and 60°N (2nd panel), for latitudes between -20° and 20°N (3rd panel) and for latitudes between -60° and -20°N (bottom panel). When performing averages over all latitudes and longitudes, i.e. for the entire globe (upper panel), the agreement is excellent. Maxima and minima showing CO seasonality are the same for IASI and MOPITT even if some small differences in magnitude can appear. Looking at the other latitude bands (40° width), the best agreement is noticed in the Southern Hemisphere (60°S-20°S), where the CO concentrations are the smallest, with mainly oceans and no sources. In the Northern Hemisphere, where most of the urban areas are, leading to important anthropogenic sources, the CO concentrations are the largest (compared to the other latitude bands). Finally, the larger differences can be observed in the Tropics (-20°; 20°N), IASI concentrations being larger than the MOPITT's one. The cloud cover and the smaller swath size lead to low MOPITT observation count over the Tropics. IASI and MOPITT have different cloud screening algorithms. Also there are globally less MOPITT data than IASI ones, because of the size of the MOPITT swath (section 1.3)[1].

[1] For example, around the TCCON station in the Philippines, Burgos (18.53 N, 120.65 E) and over the period 2017-2021, MOPITT had between 0 and 20 (max) observations per month, whereas IASI had between 30 and 130 measurements. TCCON had between 100 and 1400 observations per month.

More generally, these results are in agreement with Buchholz et al. (2021) who show also the excellent agreement between MOPITT and IASI, when comparing the CO L3 in the Northern and Southern hemispheres.

We also note the excellent agreement between the different IASI instruments and the fact that the ICDR time series from Metop C is in accordance with the CDR one, and an excellent completion of it.

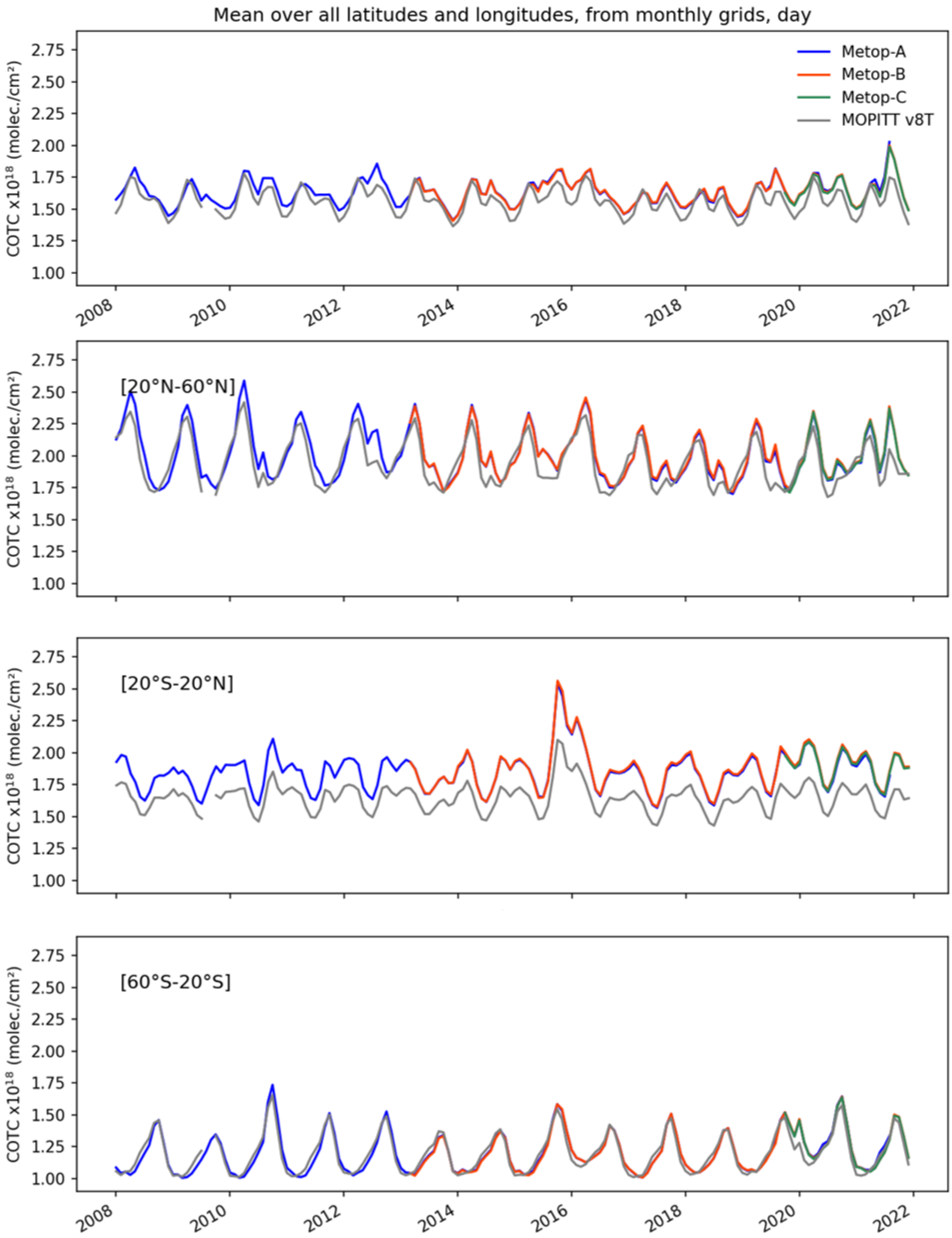

Figure 7: Averages of daytime CO concentrations over different latitude bands: for the entire globe (top), for latitudes between 20° and 60°N (2nd panel), for latitudes between -20° and 20°N (3rd panel) and for latitudes between -60° and -20°N (bottom). For IASI-A in blue, IASI-B in red, IASI-C in green and MOPITT in grey.

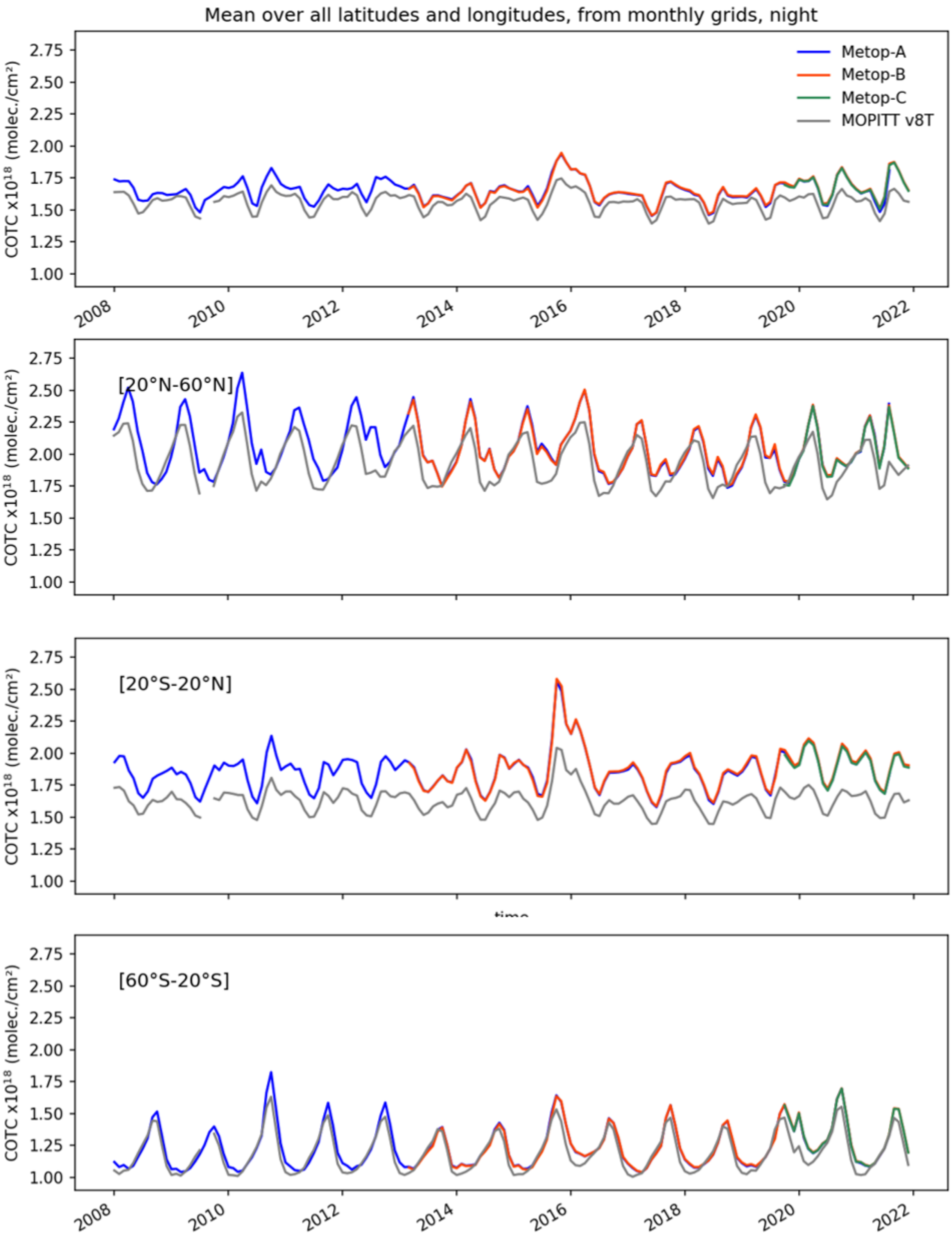

Figure 8: Same as Figure 7 but for nighttime data.

As said in Section 1.2, IASI CO L3 products include error grids, that characterize the CO retrievals. These error grids cannot be validated against other sensor's products. We show time series of averaged errors over different latitude bands in Figure 9 (daytime) and Figure 10 (nighttime). We can appreciate the excellent consistency between the A, B and C products. Comparing Figure 9 (daytime) and Figure 810 (nighttime), we see that CO errors during the night are larger than CO errors during the day, in particular in the Northern Hemisphere. Note that IASI-A CO error is larger than for IASI-B and C starting mid-2019 (beginning of end of life of IASI-A), especially in the Southern

Hemisphere during daytime (see lower panel of Figure 9) and in the Northern Hemisphere during nighttime (second panel of Figure 10).

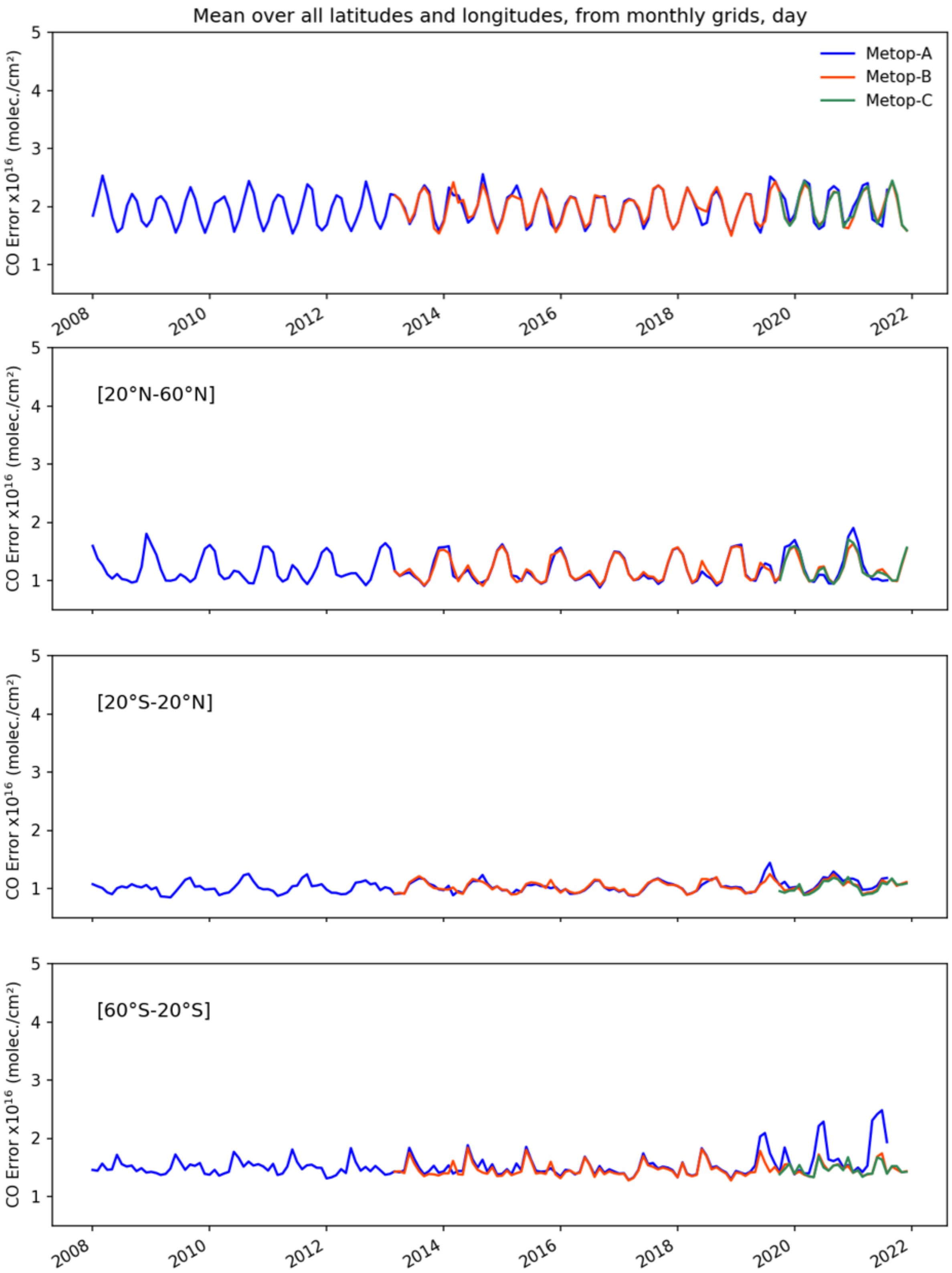

Figure 9: Averages of daytime CO errors corresponding to CO retrievals over different latitude bands: for the entire globe (top), for latitudes between 20° and 60°N (2nd panel), for latitudes between -20° and 20°N (3rd panel) and for latitudes between -60° and -20°N (bottom). For IASI-A in blue, IASI-B in red and IASI-C in green.

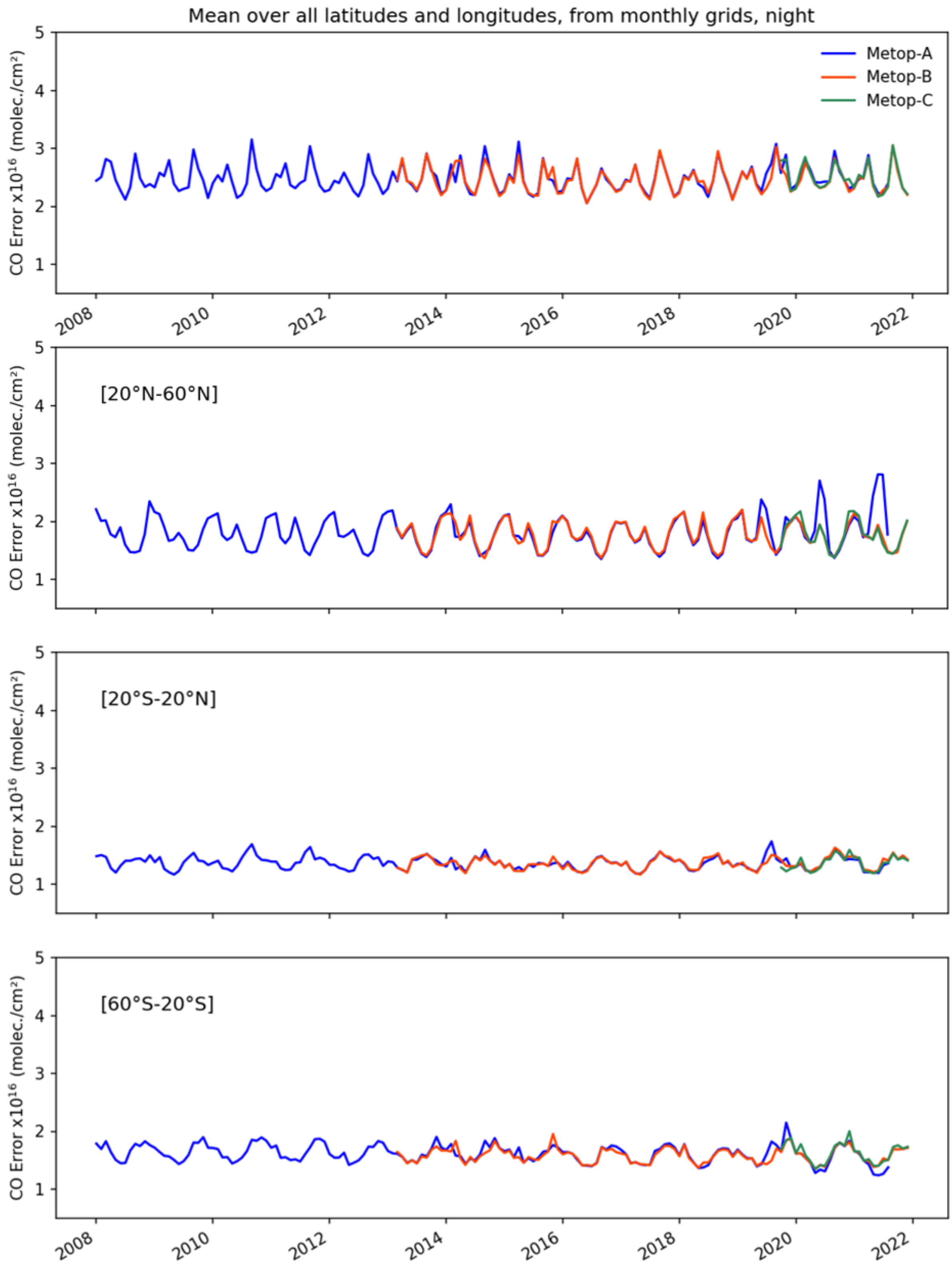

Figure 10: Same as Figure 9 but for nighttime data.

2.4 Regional and city scale comparison

Looking at smaller scales, averages are performed over eighteen different regions (see Figure 11). Thirteen are 5°x5° boxes and five are 2°x2° boxes around cities. The list of the different regions/boxes, with latitude/longitudes bonds is given in Table 1.

Time series of these averages (for both daytime and nighttime) are presented in Figure 12 to Figure 17**Erreur ! Source du renvoi introuvable.** for IASI-A, Figure 18 to Figure 23 for IASI-B and Figure 24 to Figure 29 for IASI-C.

Biases in % are calculated as follow:

$$100 \times \frac{CO_{IASI} - CO_{MOPITT}}{CO_{MOPITT}}$$

For the 18 regions, we see that seasonal cycles are well captured and are in good agreement for the two instruments. Large CO concentrations are observed in the China region, due to anthropogenic activities (industry, traffic, heating). Seasonality is well seen, and is well captured by IASI and MOPITT. On average over the 14 years (2008-2021, IASI-A), bias is -1.2% with a standard deviation of 11.7 [inside the brackets on the figures]. During nighttime, mean bias is larger: -15.9% [7.4]. During the winter months, IASI concentrations are usually smaller than the MOPITT ones. This can be explained by the different a priori information used as input in the retrieval algorithms (MOPITT uses a variable a priori with time and location, IASI uses a fixed one – section 1.3, and detailed in George et al. 2015). Also, auxiliary variables needed in the optimal estimation scheme such as emissivity, cloud coverage, temperature and humidity information, play an important role in the retrievals, and can explain the differences. Emissivity assumptions are particularly important during the winter over ice/snow covered areas. Some further work is needed to quantify the part of the apriori's choice and the part of the auxiliary variables to explain this difference, for the China but also for Canada and Moscow, where large biases can be observed. At first glance, China monthly biases are getting worse in the later years (after 2017), this needs to be further investigated.

Other regions are affected by the different a priori's: Canada, Siberia and Moscow, all in the Northern Hemisphere, with biases of -6.9% [11.3], -4.9% [10.5] and -7.4% [10.3] (for IASI-A) respectively. This can also be noticed over Eastern-USA and Europe with biases of -5.5% [3.9] and -3.9% [6] (for IASI-A) respectively. During nighttime, Canada, Siberia and Moscow biases are lower in absolute value: 1.5% [10.8], -1.4% [13.2, and -5.3% [11.4] respectively. For Eastern-USA and Europe, biases are: -10% [5.2] and -1.2% [7].

The biomass burning in Africa caused by farmers for agricultural cleaning shows the largest maxima and minima. This seasonality for large CO concentrations is extremely well captured by both IASI and MOPITT. Mean bias of 9.2% with a standard deviation of 7.9, for IASI-A, is one of the largest for daytime measurements (12.6% [8.5] for IASI-B). For nighttime, the same order of magnitude is observed: 8.6% for the mean bias with a standard deviation of 15 for IASI-A (10.6% [16] for IASI-B).

The smallest CO concentrations are observed in the Pacific region, away from the sources. Biases are 5.1% [5.1] for IASI-A and 6.3% [5.4] for IASI-B. Note the anomaly in January 2020 when both IASI and MOPITT capture larger CO concentrations than usual: this is due to the extremely intense Australian fires.

For IASI-C/MOPITT comparison, the time series cover 27 months. An excellent agreement between IASI's and MOPITT is observed in Figure 24 to Figure 29. Evaluating the average biases for IASI-C with respect to MOPITT can be tricky as the considered time period is short. In the future, more data points will help better explain the average bias between the two.

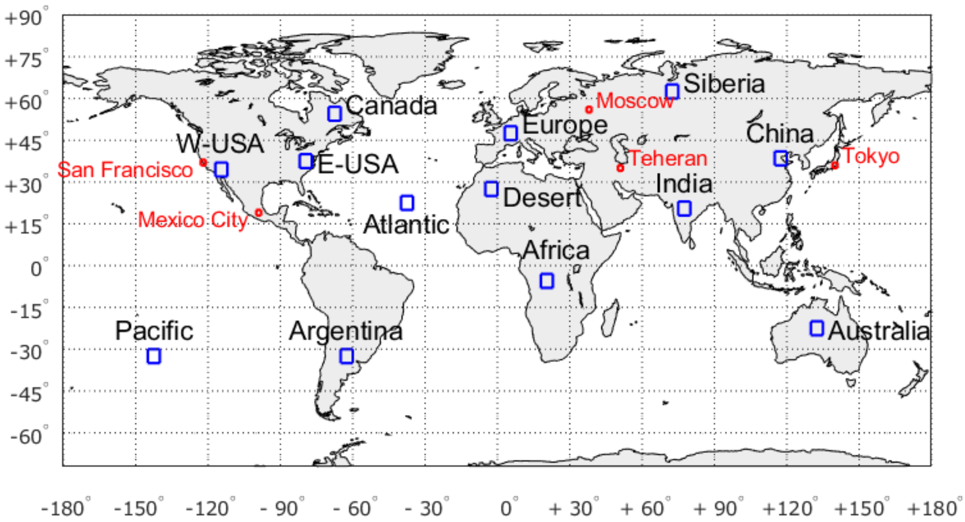

Figure 11: Location of the different regions chosen for the validation. Five 2°x2° boxes around cities are plotted in red. Thirteen 5°x5° boxes (in blue) are distributed over the globe.

Table 1: Name and localization (latitude; longitude) of the eighteen selected regions.

Name of the region	Latitude bounds (°N)	Longitude bounds (°E)
Siberia	60, 65	70, 75
Canada	52, 57	-70, -65
Europe	45, 50	3, 8
Eastern-USA (E-USA)	35, 40	-82, -77
Western-USA (W-USA)	32, 37	-117, -112
China	36, 41	115, 120
Desert	25, 30	-5, 0
Atlantic	20, 25	-40, -35
India	18, 23	75, 80
Africa	-8, -3	18, 23
Australia	-25, -20	130, 135
Argentina	-35, -30	-65, -60
Pacific	-35, -30	-145, -140
Moscow	55, 57	37, 39
San Francisco	36, 38	-123, -121

Teheran	34, 36	50, 52
Tokyo	35, 37	139, 141
Mexico city	18, 20	-100, -98

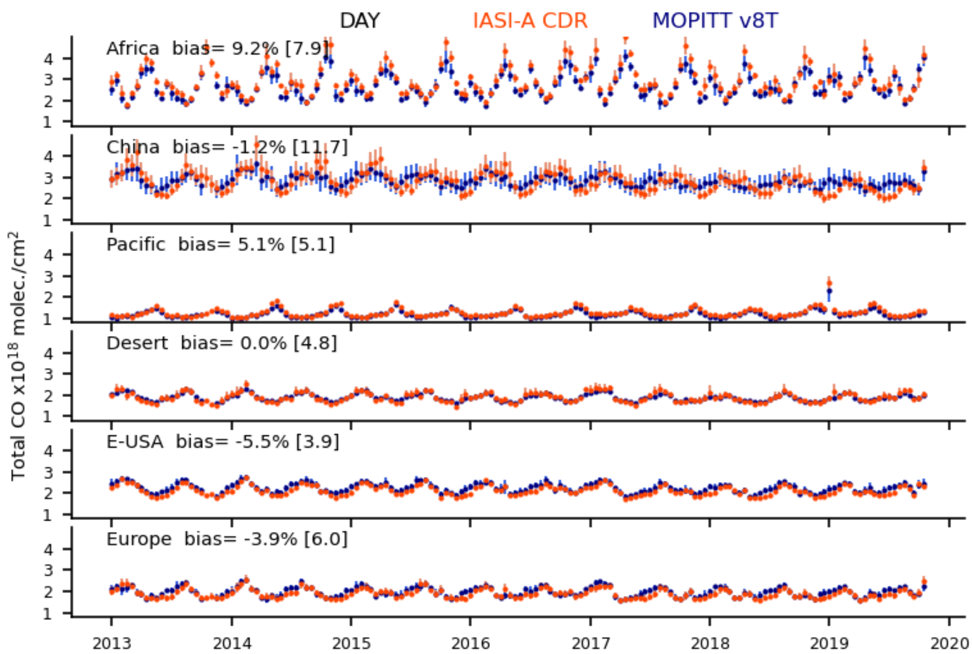

Figure 12: Daytime time series of averages in six selected regions (Africa, China, Pacific, Desert, Eastern United states (noted E-USA) and Europe) for IASI-A in red and MOPITT in blue. Vertical bars represent the variability within the boxes. Mean bias as well as standard deviation (in square brackets) are calculated and listed for each region.

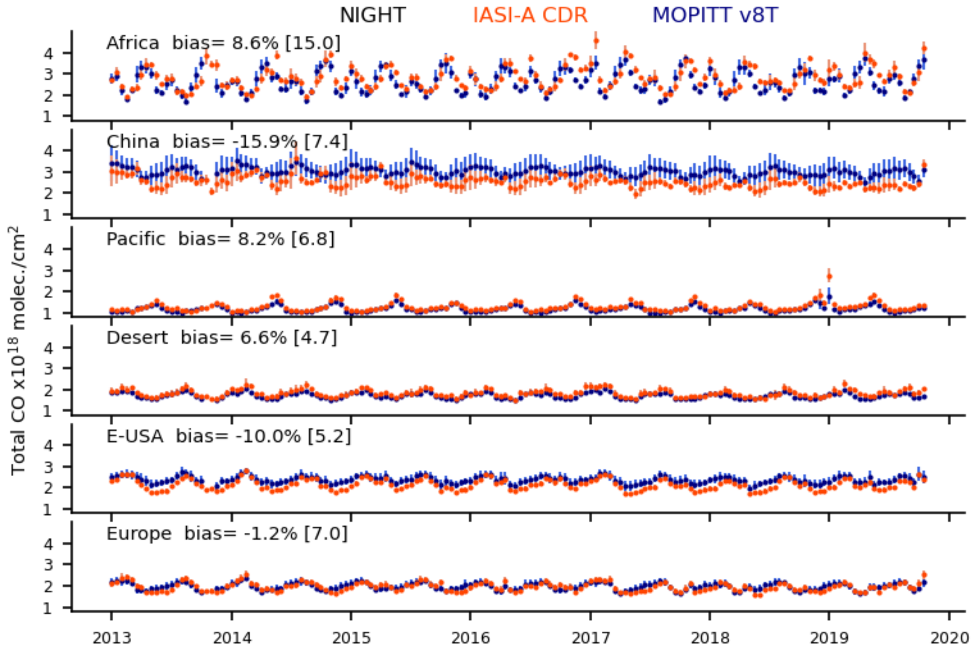

Figure 13: Same as Figure 12 but for nighttime data.

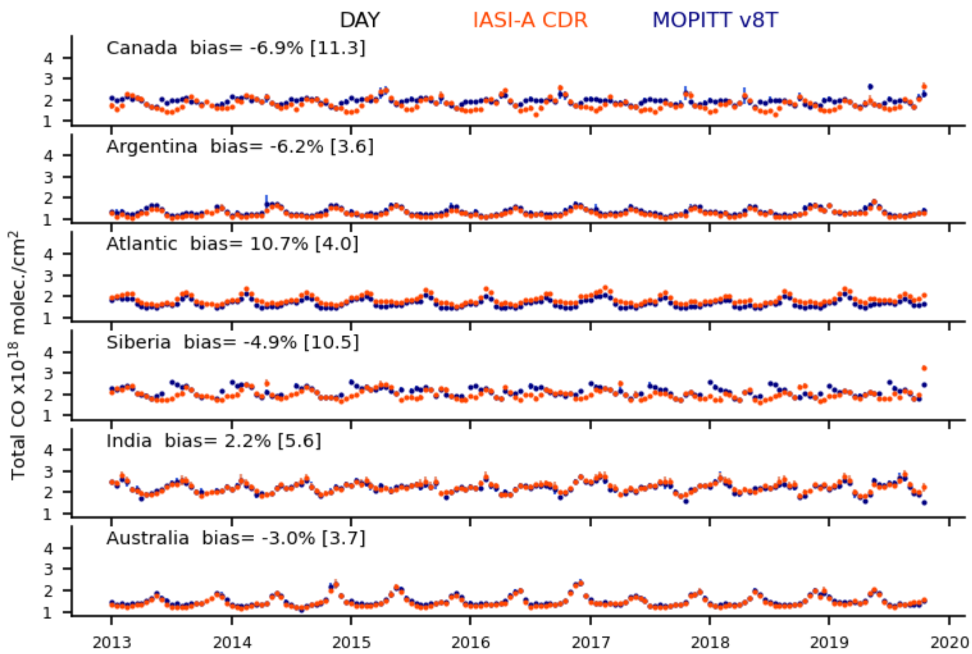

Figure 14: Same as Figure 12 but for six other regions: Canada, Argentina, Atlantic, Siberia, India and Australia.

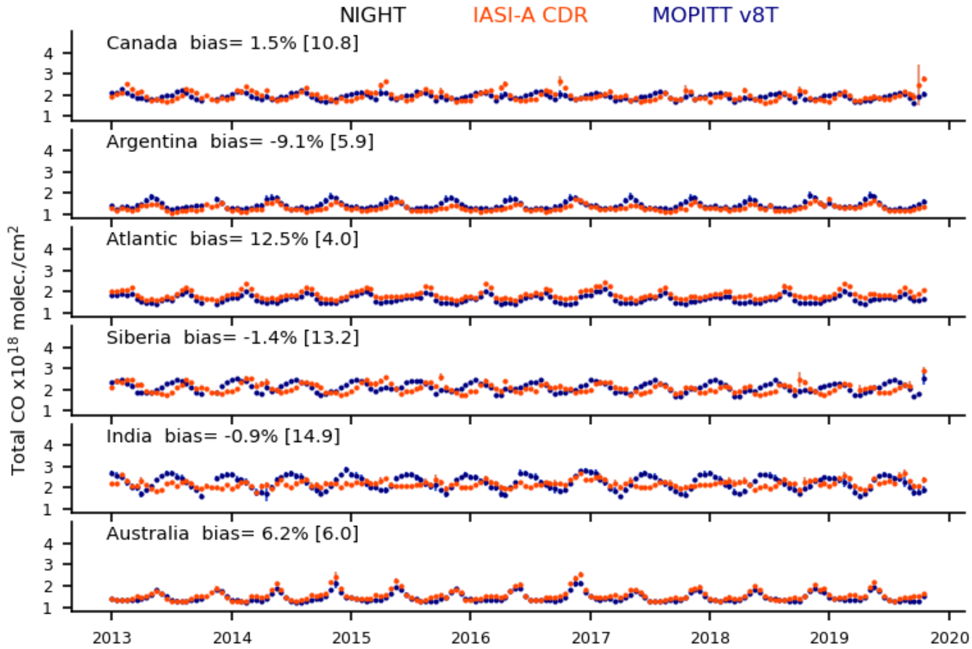

Figure 15: Same as Figure 12 but for nighttime data for six other regions: Canada, Argentina, Atlantic, Siberia, India and Australia.

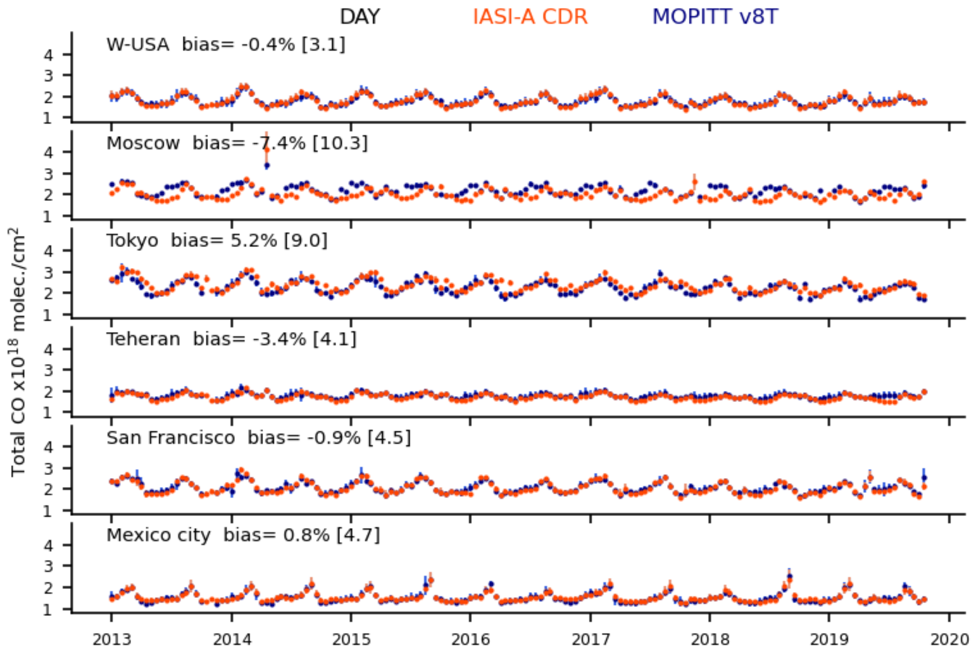

Figure 16: Same as Figure 12 but for six other regions: Western-United States (noted W-USA), Moscow, Tokyo, Teheran, San Francisco and Mexico city.

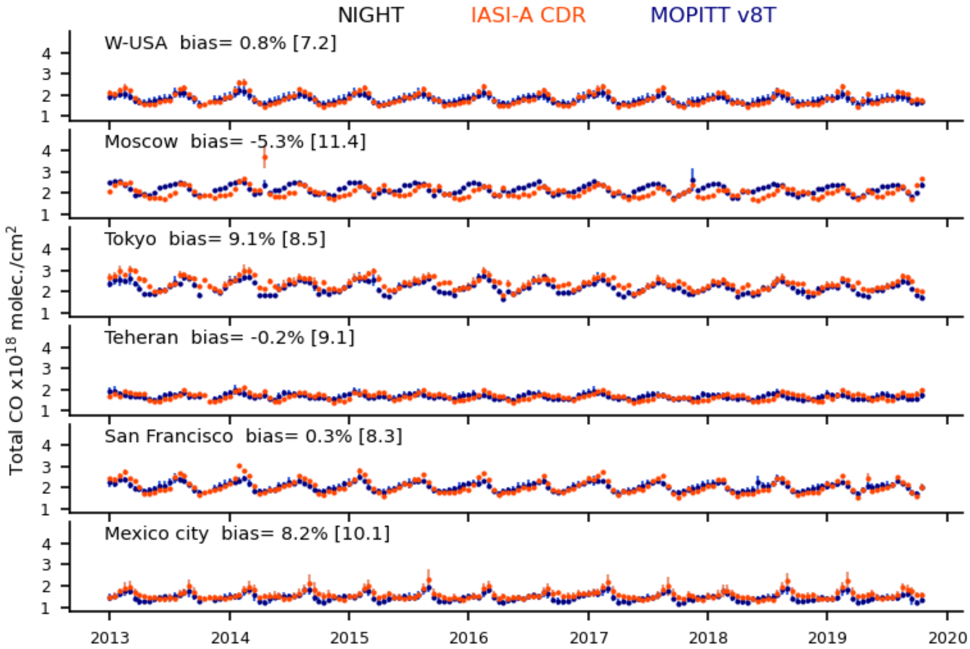

Figure 17: Same as Figure 12 but for nighttime date for six other regions: Western-United States (noted W-USA), Moscow, Tokyo, Teheran, San Francisco and Mexico city.

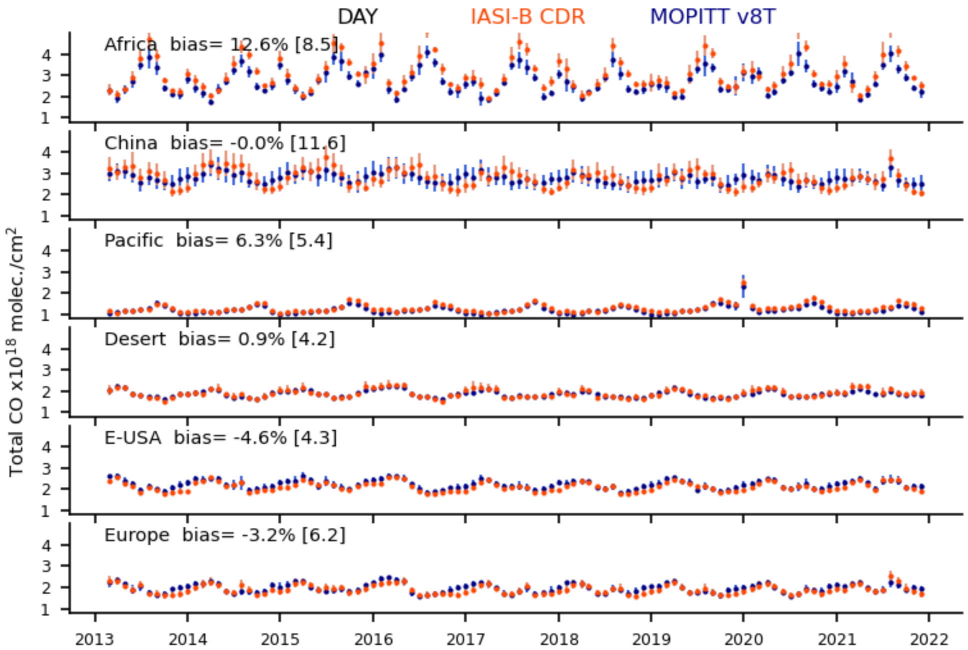

Figure 18: Same as Figure 12 but for IASI-B.

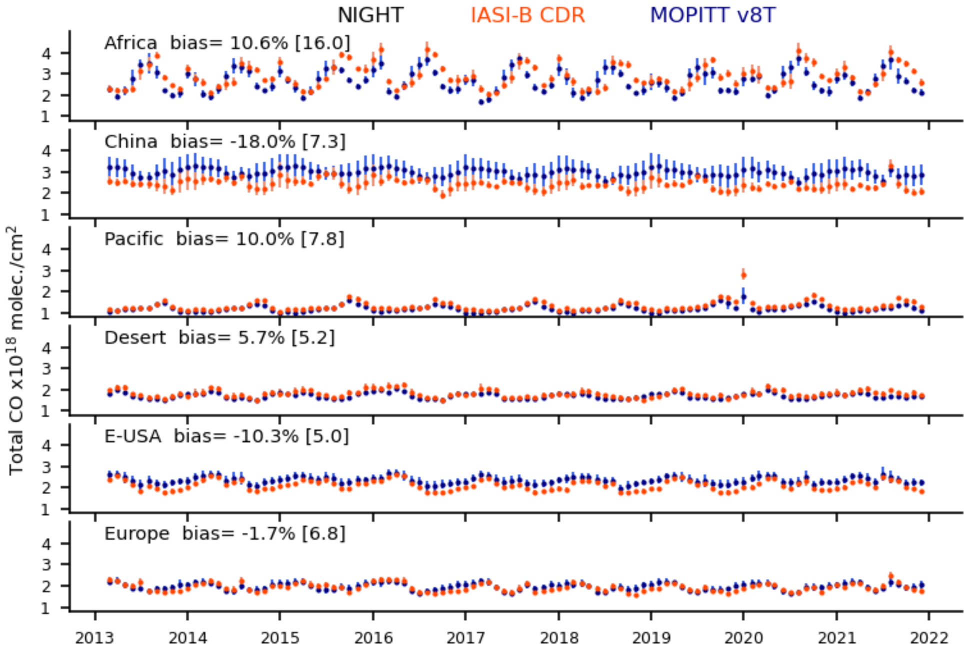

Figure 19: Same as Figure 12 but for IASI-B nighttime data.

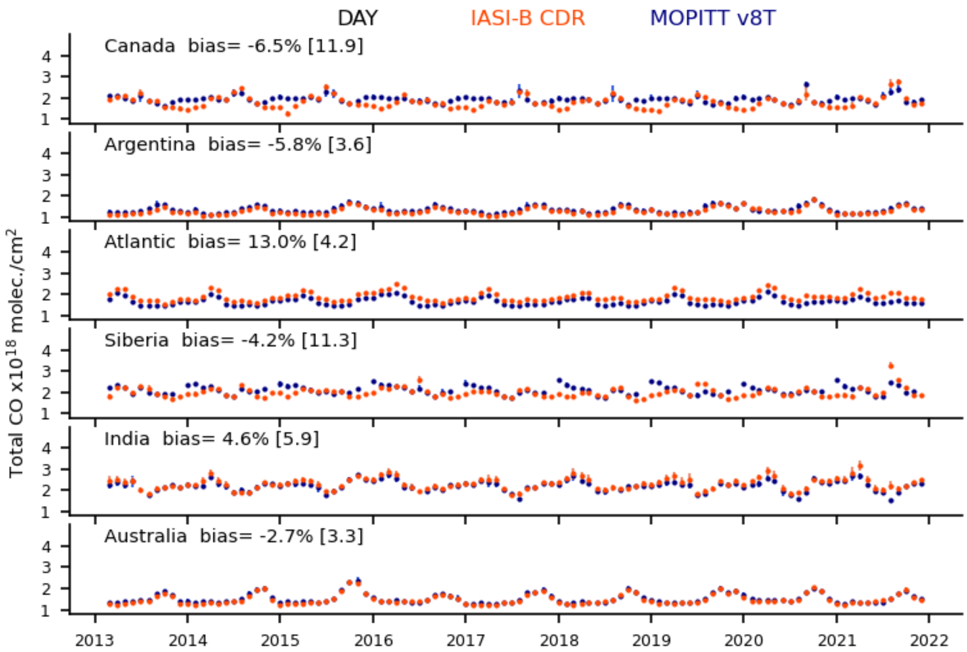

Figure 20: Same as Figure 12 but for IASI-B, for six other regions: Canada, Argentina, Atlantic, Siberia, India and Australia.

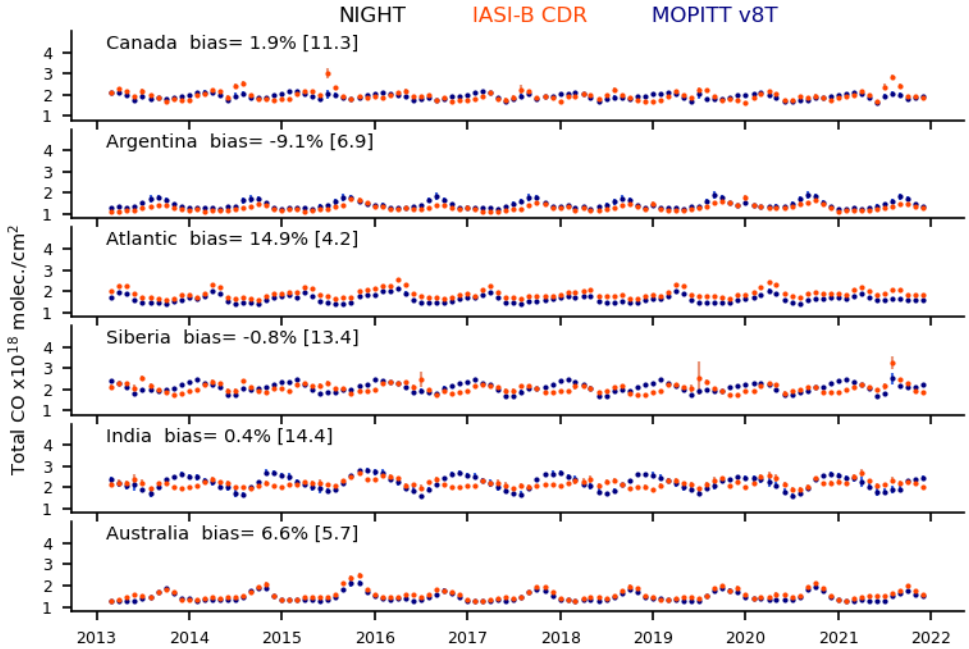

Figure 21: Same as Figure 12 but for IASI-B nighttime data, for six other regions: Canada, Argentina, Atlantic, Siberia, India and Australia.

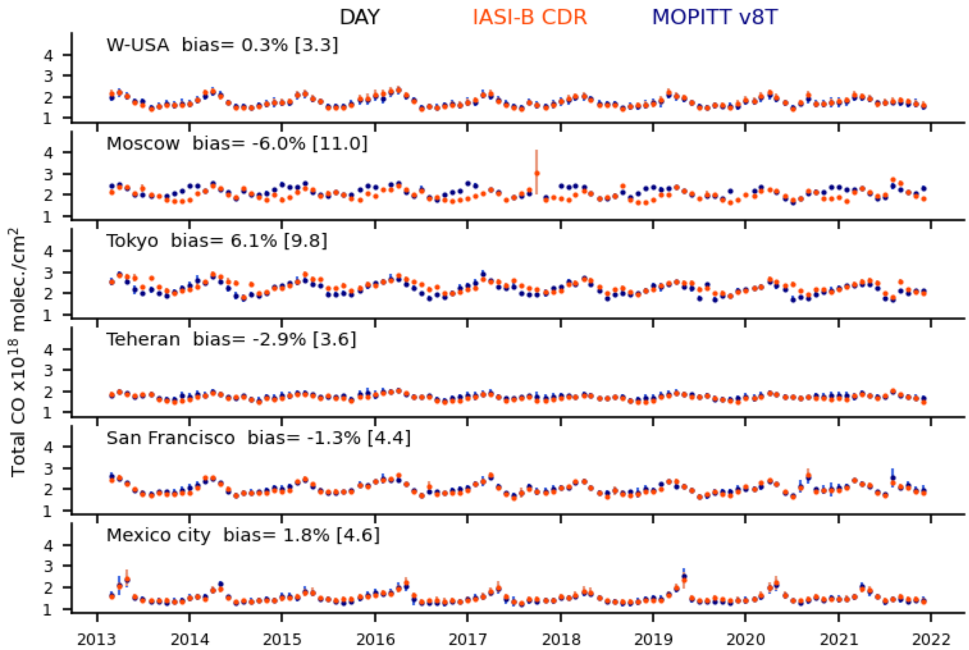

Figure 22: Same as Figure 12 but for IASI-B, for six other regions: Western-United States (noted W-USA), Moscow, Tokyo, Teheran, San Francisco and Mexico city.

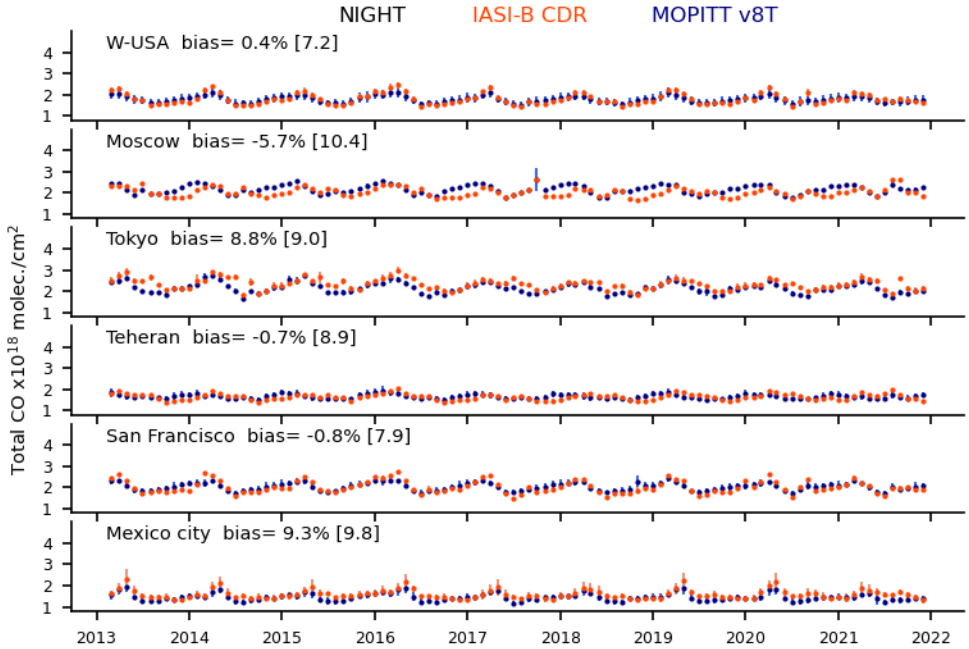

Figure 23: Same as Figure 12 but for IASI-B nighttime data, for six other regions: Western-United States (noted W-USA), Moscow, Tokyo, Teheran, San Francisco and Mexico city.

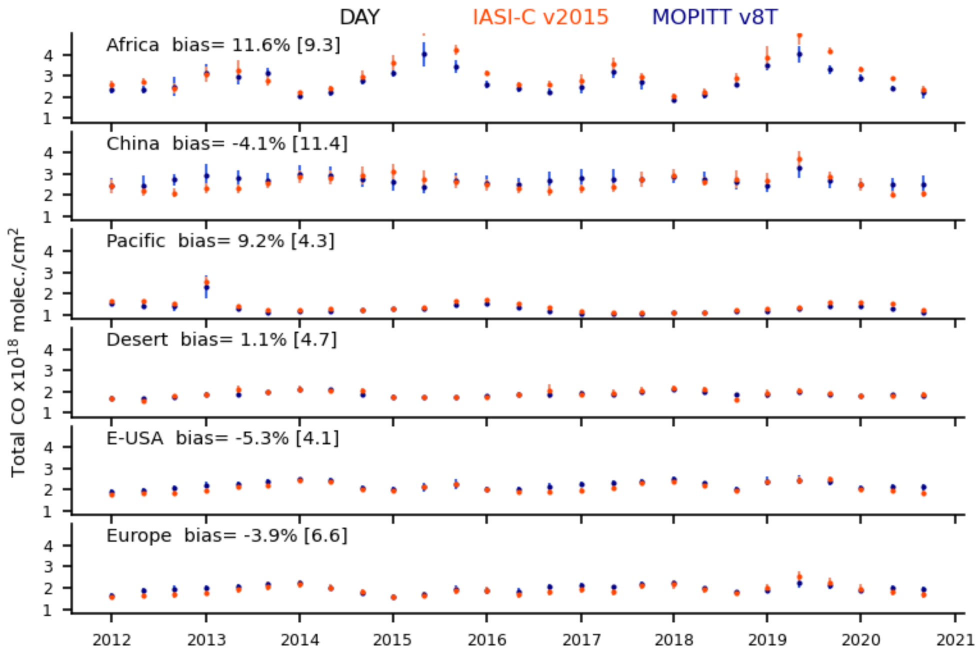

Figure 24: Same as Figure 12 but for IASI-C.

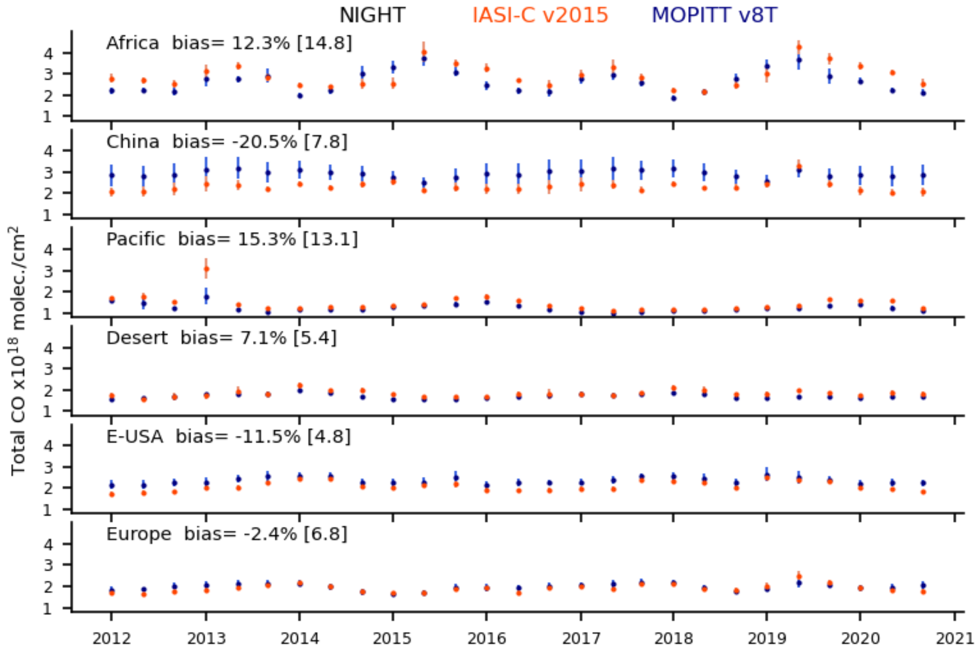

Figure 25: Same as Figure 12 but for IASI-C nighttime data.

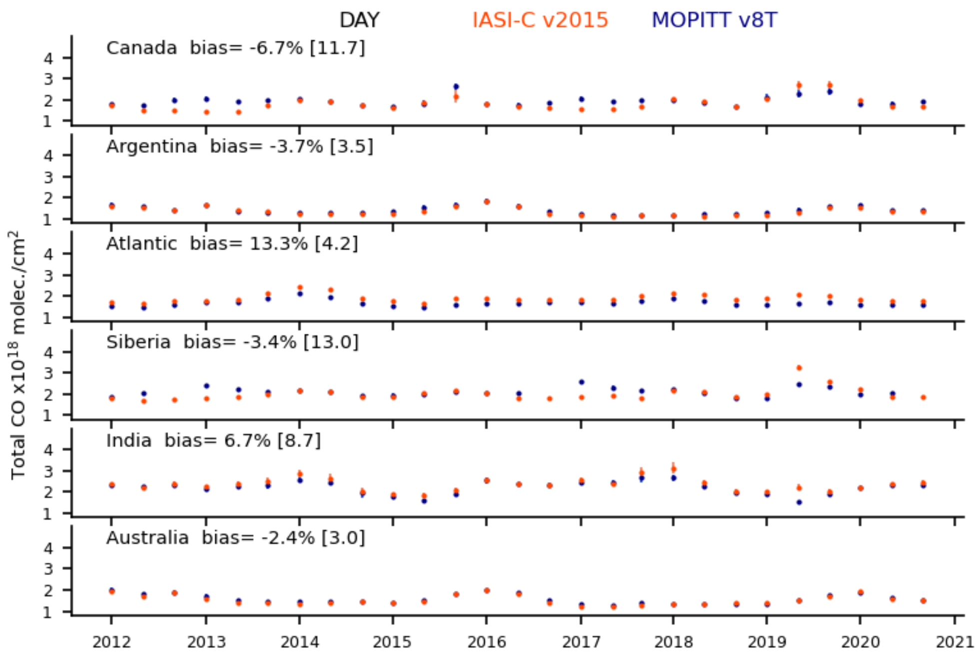

Figure 26: Same as Figure 12 but for IASI-C, for six other regions: Canada, Argentina, Atlantic, Siberia, India and Australia.

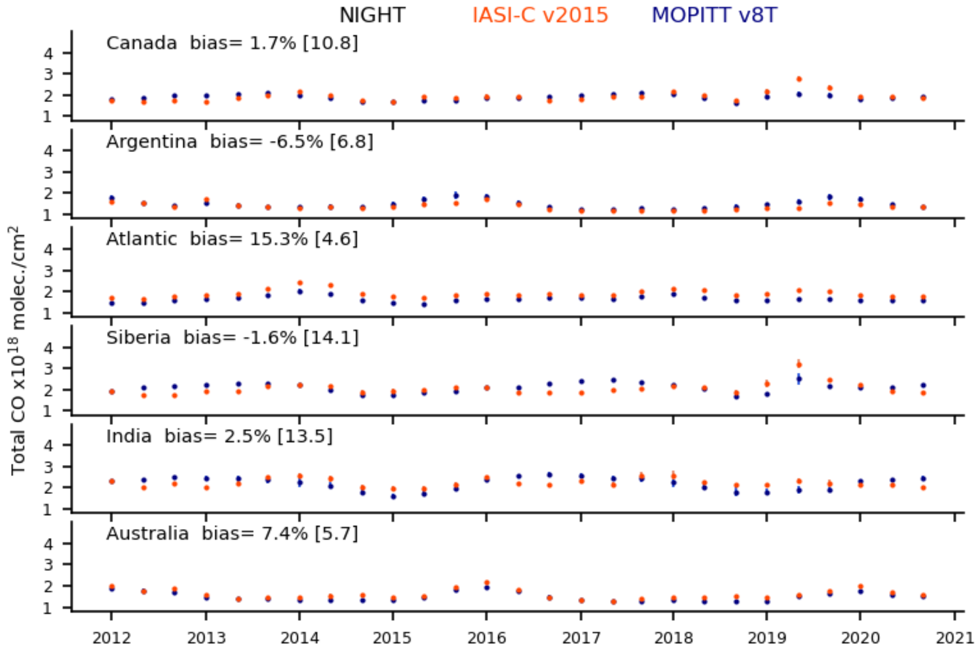

Figure 27: Same as Figure 12 but for IASI-C nighttime data, for six other regions: Canada, Argentina, Atlantic, Siberia, India and Australia.

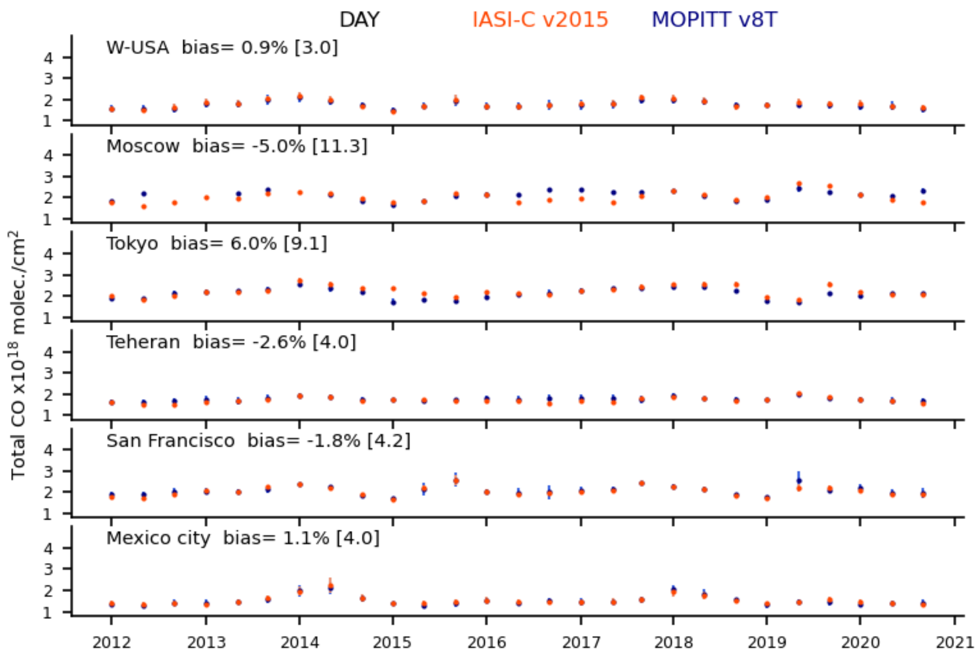

Figure 28: Same as Figure 12 but for IASI-C, for six other regions: Western-United States (noted W-USA), Moscow, Tokyo, Teheran, San Francisco and Mexico city.

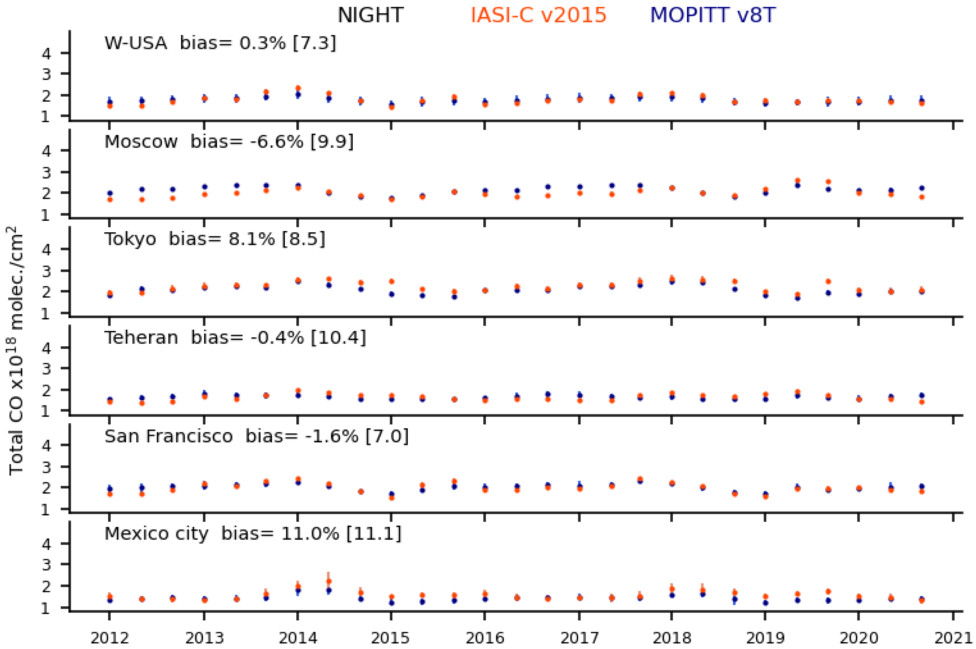

Figure 29: Same as Figure 12 but for IASI-C nighttime data, for six other regions: Western-United States (noted W-USA), Moscow, Tokyo, Teheran, San Francisco and Mexico city.

CONCLUSION

In this validation report, we compared IASI-A, B CDR and IASI-C ICDR L3 products with MOPITT CO L3 products. Qualitative spatial comparison has been performed in Section 1 as well as quantitative comparison for different latitude bands in Section 2 and different regions as well as cities in Section 3. Results are very satisfactory, showing generally a good agreement between the two products. Seasonality is very well captured for all the regions. Daytime mean biases for IASI-A/MOPITT comparison range between -6.9% [11.3] and 10.7% [4] for the 5°x5° regions and between -7.4% [10.3] and 5.2% [9] for the five cities (2°x2° boxes). For nighttime, mean biases range between -15.9% [7.4] and 8.6% [15] for the 5°x5° regions and between -5.3% [11.4] and 9.1 [8.5] for the five cities. For IASI-B/MOPITT, daytime mean biases range between -6.5% [11.9] and 13% [4.2] for the 5°x5° regions and between -6% [11] and 6.1% [9.8] for the cities. For nighttime, IASI-B/MOPITT mean biases are slightly larger in absolute value, ranging between -18% [7.3] and 14.9% [4.2] for the 5°x5° regions and between -5.7% [10.4] and 9.3 [9.8] for the cities. For IASI-C/MOPITT comparison, mean biases are sometimes less good but should be looked at with caution as the considered time period is relatively short (27 months): between -6.7% [11.7] and 13.3% [4.2] in the 5°x5° regions and between -5% [11.3] and 6% [9.1] for the cities, for daytime measurements. For nighttime, mean biases range between -20.5% [7.8] and 15.3% [4.6] for the 5°x5° regions and between -6.6% [9.9] and 11% [11.1] for the cities. As discussed in George et al. (2015), large differences can be noticed during the winter months in the Northern hemisphere (Canada, Eastern-USA, Europe, Siberia) and are explained by the different a priori's used in the different retrieval algorithms. Also, auxiliary variables needed in the optimal estimation scheme such as emissivity, cloud coverage, temperature and humidity information, play an important role in the retrievals, and can explain the differences.

In conclusion, biases (<=13.3%) for daytime, for Metop-A, B and C, are in compliance with product requirements IASI L3 CO (For standard cases: Threshold 15%, Target 10% and Optimal 8%; for unusual cases (high pollution or low signal): Threshold 50%, Target 20% and Optimal 10%). For nighttime measurements, mean biases doesn't exceed 20.5% in absolute value, still lower than the 50% threshold of low signal cases.

Recommendations for users: In this report we presented a comparison for daytime and nighttime data. Depending on the studies/purposes, users may choose to use only daytime data. As a matter of fact, both IASI and MOPITT show a better sensitivity to the surface during the day. Note that only daytime data have been used in Buchholz et al. (2021) when studying CO trends over seventeen years. We recall here that nighttime data are robust and of good quality. The agreement with MOPITT is good. Keep in mind that CO errors during the night are larger than CO errors during the day, in particular in the Northern Hemisphere (Section 2.2).

References

Barré et al., Assessing the impacts of assimilating IASI and MOPITT CO retrievals using CESM-CAM-chem and DART, J. Geophys. Res. Atmos., 120, 10, 501–10, 529, doi:10.1002/2015JD023467, 2015.

Bouillon, M., Safieddine, S.; Hadji-Lazaro, J.; Whitburn, S.; Clarisse, L.; Doutriaux-Boucher, M.; Coppens, D.; August, T.; Jacquette, E.; Clerbaux, C. Ten-Year Assessment of IASI Radiance and Temperature. *Remote Sens.*, *12*, 2393. https://doi.org/10.3390/rs12152393, 2020.

Buchholz et al., Air pollution trends measured from Terra: CO and AOD over industrial, fire prone, and background regions, Remote Sens. of Env ., https://doi.org/10.1016/j.rse.2020.112275, 2021.

Deeter, M. N., Edwards, D. P., Francis, G. L., Gille, J. C., Mao, D., Martínez-Alonso, S., Worden, H. M., Ziskin, D., and Andreae, M. O.: Radiance-based retrieval bias mitigation for the MOPITT instrument: the version 8 product, Atmos. Meas. Tech., 12, 4561–4580, https://doi.org/10.5194/amt-12-4561-2019, 2019.

Drummond, J. R., J. Zou, F. Nichitiu, J. Kar, R. Deschambaut, and J. Hackett: A review of 9-year performance and operation of the MOPITT instrument, J. Adv. Space Res., doi:10.1016/j.asr.2009.11.019, 2010.

George, M., Clerbaux, C., Bouarar, I., Coheur, P.-F., Deeter, M. N., Edwards, D. P., Francis, G., Gille, J. C., Hadji-Lazaro, J., Hurtmans, D., Inness, A., Mao, D., and Worden, H. M.: An examination of the long-term CO records from MOPITT and IASI: comparison of retrieval methodology, Atmos. Meas. Tech., 8, 4313-4328, doi:10.5194/amt-8-4313-2015, 2015.

Hurtmans, D, Coheur, P.-F., Wespes, C, Clarisse, L., Scharf, O., Clerbaux, C., Hadji-Lazaro, J., George, M., Turquety, S.: FORLI radiative transfer and retrieval code for IASI, J. Quant. Spectrosc. Ra., 113, 1391–1408, doi:10.1016/j.jqsrt.2012.02.036, 2012.